physica status solidi b
www.pss-b.com

Nonlocal Electrical Detection of Spin-Polarized Surface Currents in the 3D Topological Insulator $BiSbTeSe_2$

*Shaham Jafarpisheh, Frank Volmer, Zhiwei Wang, Bárbara Canto, Yoichi Ando, Christoph Stampfer, and Bernd Beschoten**

The spin-polarized surface states in topological insulators offer unique transport characteristics that make them distinguishable from trivial conductors. Herein, the impact of these surface states in the topological insulator $BiSbTeSe_2$ is detected by electrical means using a nonlocal (NL) transport configuration with ferromagnetic Co/Al_2O_3 electrodes. It is shown that the NL measurement allows probing of the surface currents flowing along the whole surface, i.e., from the top along the side to the bottom surface and back to the top surface along the opposite side. Increasing the temperature increases the interaction between bulk and surface states, which shortens this NL current path along the surface and hence leads to a complete disappearance of the NL signal at around 20 K. Interestingly, it is observed that the ratio between spin signal to background signal is much larger in the NL geometry compared to the local one. Given that the observed ratio in the NL geometry aligns well with expectations for spin-polarized surface states, the findings suggest that an as-yet unresolved mechanism diminishes the spin signal in the local geometry.

1. Introduction

Topological surface states (TSS) and 2D electron gases (2DEG) can coexist at the surface of 3D topological insulators (TIs),[1–3] whereas the TSS exhibit spin-momentum locking, the 2DEG is characterized by bands with pronounced Rashba spin splitting.[4] Under an electrical bias voltage, the spin textures of these surface states lead to a current-induced spin polarization (CISP), where the polarization is perpendicular to the momentum direction, however with different signs between the TSS and Rashba-split states (RSS).[5–9] Therefore, both TSS and RSS offer many opportunities for spintronics and magnetoelectronics.[9–12] For such purposes, spin-sensitive ferromagnetic electrodes can be used to indirectly detect the spin-polarized surface currents, as these currents create a difference in the electrochemical potentials for spins parallel and antiparallel to the magnetization direction of the electrodes.[13–15] Therefore, reversing either the magnetization direction of the ferromagnetic electrodes by an external magnetic field or reversing the flow direction of the current lead to a sign reversal in the magnetic hysteresis loop of the detected spin signal. This behavior has indeed been observed in several studies before.[8,9,13,16–24]

However, so far the amplitudes of reported spin signals in local measurement geometries are surprisingly small for allegedly fully polarized surface currents and are additionally superimposed by magnetization independent background signals that are two to three orders of magnitude larger than the spin signal.[8,13,16–20] One possible explanation for such diminished spin signals are invasive contacts that might disturb the spin-polarized surface states.[25–29] Another explanation might be possible contributions from transport over bulk and/or defect states in the local transport geometry (black arrows in **Figure 1**a,b).[30–35] Charge transport over such states, especially in the presence of magnetic fringe fields, can also show similar

S. Jafarpisheh, F. Volmer, C. Stampfer, B. Beschoten
2nd Institute of Physics and JARA-FIT
RWTH Aachen University
52074 Aachen, Germany
E-mail: bernd.beschoten@physik.rwth-aachen.de

S. Jafarpisheh, C. Stampfer
Peter Grünberg Institute (PGI-9)
Forschungszentrum Jülich
52425 Jülich, Germany

The ORCID identification number(s) for the author(s) of this article can be found under https://doi.org/10.1002/pssb.202500313.

DOI: 10.1002/pssb.202500313

Z. Wang, Y. Ando
Physics Institute II
University Cologne
50937 Cologne, Germany

Z. Wang
Key Laboratory of Advanced Optoelectronic Quantum Architecture and Measurement, School of Physics
Beijing Institute of Technology
Beijing 100081, P. R. China

B. Canto
AMO GmbH, Gesellschaft für Angewandte Mikro- und Optoelektronik
52074 Aachen, Germany

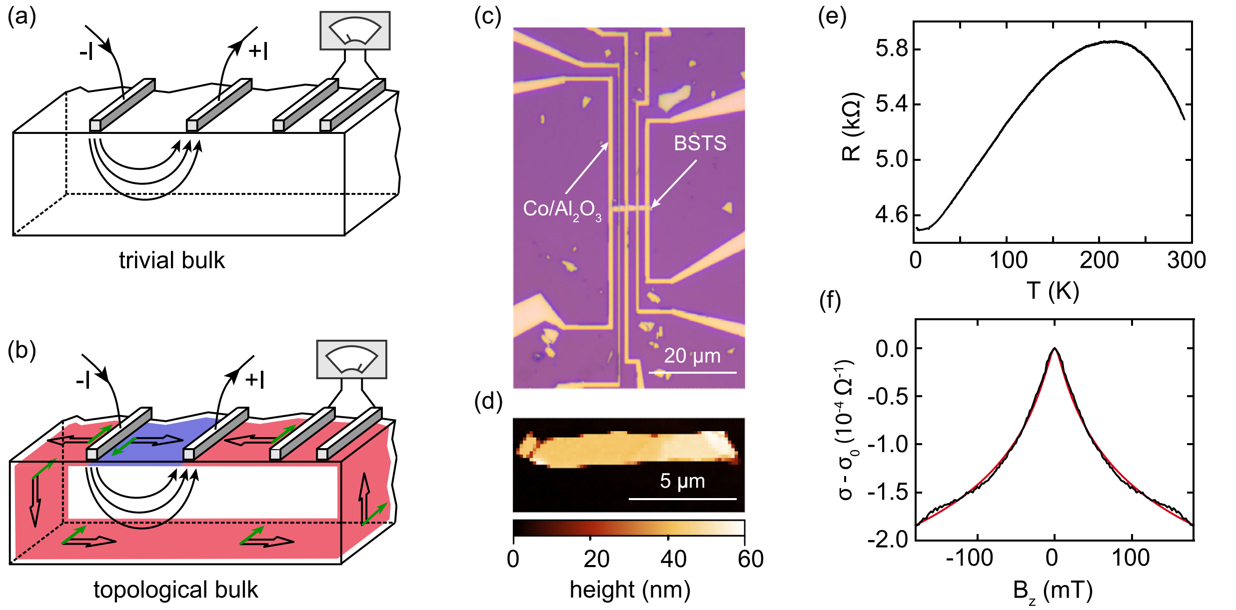

Figure 1. a) Distribution of the current inside the bulk of a material with trivial band structure (black arrows). Only a negligible amount of current due to the effect of current spreading is expected under the nonlocal detection electrodes. b) Distribution of the current inside a 3D topological insulator. Depicted are the potentially present bulk channel (black arrows), the local surface channel directly between source and drain (blue), and a second surface channel (red), which connects source and drain in a nonlocal manner. The spin polarization directions are indicated by green arrows and correspond to the case where spin-momentum–locked transport carried by the TSS dominates over transport via the RSS. c) Optical image of the 40 nm thick exfoliated BSTS flake contacted with Co/Al_2O_3 electrodes. d) AFM scan of the flake shown in panel (c) before electrode fabrication. e) Four-probe resistance as a function of temperature. f) Weak antilocalization measurement at a base temperature of $T = 3$ K as a function of an out-of-plane magnetic field B_z. The red line is a fit using the Hikami–Larkin–Nagaoka model.

magnetic field dependent transport signatures compared to the signatures attributed to the TSS or RSS.[8,36,37] This can be a problem in local measurements of the surface states in-between source and drain contacts (transport over these surface states is depicted by the blue area in Figure 1b). However, the topologically protected surface states as well as the RSS are expected to fully enclose the 3D bulk connecting all facets of a strong TI.[38] If surface states on the one hand and bulk and defect states on the other hand are sufficiently decoupled, a third transport channel therefore opens from source to drain, carrying the current nonlocally along the surface (see red current path in Figure 1b).[39–42] A nonlocal (NL), spin-sensitive voltage measurement of this second surface transport channel thus offers, in principle, a way to separate the contributions from surface states on the one hand and bulk and/or defect states on the other hand.

In this work, we investigate both local (L) and NL electrical transport measurements of the surface states in exfoliated $BiSbTeSe_2$ (BSTS) flakes.[43] And indeed, we observe distinctive different spin transport properties in these two configurations. On the one hand, the ratio between the spin signal and the background signal is nearly two orders of magnitude higher in the NL geometry compared to the local geometry, the latter being consistent with values reported in the literature. This hints to the fact that so far an unknown phenomena diminishes the spin signal in the local geometry. On the other hand, we observe significantly different temperature dependencies between local and NL spin signals. Thermally activated hopping transport is likely the reason for the different temperature dependencies, as the NL current path is shortened by this temperature activated channel.

The BSTS flakes were prepared by mechanical exfoliation onto Si^{++}/SiO_2(300 nm) substrates. Tunnel-barriers were fabricated by evaporation of an aluminum (Al) seed layer (≈1 nm) over the whole flake which got naturally oxidized, followed by thermal atomic layer deposition (ALD) with tri-methylaluminum (TMA) and water as precursors for an additional ≈1 nm Al_2O_3. Here, the ALD process was used to close pinholes in the naturally oxidized Al_2O_3 layer. In the next step, e-beam lithography and e-beam evaporation was used to fabricate the cobalt (Co) electrodes. An optical image of the device together with an atomic force microscope (AFM) image of the BSTS flake after exfoliation are shown in Figure 1c,d, respectively. The thickness of the flake is ≈40 nm.

The temperature dependent resistance of the device, measured in a four-probe configuration, shows a semiconducting behavior at high temperatures and a transition to a metallic regime at $T = 200$ K (see Figure 1e). This transition corresponds to the depletion of impurity and defect bands within the bulk bandgap.[44] The metallic behavior, on the other hand, indicates surface transport that persists down to low temperatures. As it is depicted in Figure 1f, a low-field magneto-resistance measurement at $T = 3$ K shows the cusp-like feature resulting from weak antilocalization (WAL).[45–49] The existence of WAL in TIs is a hallmark of the strong spin-orbit coupling. We use the Hikami–Larkin–Nagaoka model[50,51] for fitting the WAL curve (see red trace in Figure 1f) and extract a phase coherence length of around 240 nm.

In order to probe the spin-polarized surface states, we now focus on transport measurements in both local and NL detection geometries (see **Figure 2**a,d, respectively), using spin-sensitive ferromagnetic electrodes to allow for potentiometric detection.[6] For this we apply in-plane magnetic fields along the y-direction to reverse the magnetization directions ($\vec{M}$) of the Co electrodes. We observe well-defined hysteresis loops in both local and NL configurations which are expected when the contacts are magnetized either parallel or antiparallel to the spin polarization ($\vec{S}$) of the surface charge carriers (Figure 2b,c,e,f). These measurements were conducted by applying a DC current of $\pm 1\,\mu$A between source (S) and drain (D) electrodes. After the subtraction of a background signal, which will be discussed further below, we normalize the measured voltage with the applied current between source and drain to acquire the local and NL resistances depicted in Figure 2b,c,e,f. In case of small currents as used in our measurements, it was shown that the spin-related voltage signal scales linearly with the applied current, before it saturates in some studies towards very high currents, possibly due to Joule heating or voltage-dependent population of non-surface states.[8,9,13,16,17,19,20,22] Within this linear range, calculating the local and NL resistances is therefore an easy way to compare results from different studies, which normally report on local spin signals in the range of a few mΩ to 10 Ω.[8,9,13,16–24] The quite large spin signals of around 10 Ω in the local transport geometry in our study (see Figure 2b,c) therefore belong to the highest spin signals reported in literature so far.

Important contributors to this large spin signal are the optimized tunnel barriers that show contact-resistance–area products of around 20–30 k$\Omega\mu$m^2. This is in the same range in which previous studies both on TIs [21] and graphene[52] have demonstrated increased spin signals due to increased spin injection/detection efficiencies and reduction of contact-induced spin relaxation processes. Furthermore, we note that in contrast to most other studies all of our contacts are ferromagnetic, including the source and drain contacts. This might be important because the TSS is not expected to be 100% spin-polarized, despite its spiral nature. This is due to spin-orbit interactions and a possible penetration of the TSS into subsurface layers, where fluctuating electric fields can result in complex spin textures.[53–57] Furthermore, it is the topic of ongoing research how electrical contacts to the TI affect both TSS and RSS.[25–29] Overall, it is very likely that both spin up and down transport channels have to be considered even for the TSS.[15] Accordingly, there is the possibility that in our study the use ferromagnetic source and drain electrodes might boost the spin polarization within the surface states and therefore the spin signal.

Consistent to surface state transport, we observe that reversing the electrons' momentum direction ($\vec{k}$) leads to a reversal of the spin polarization direction of the surface carriers and therefore the reversal of the respective hysteresis curves in both the L and the NL configurations (compare left and right panels in Figure 2b,c,e,f). We note that we cannot draw any definitive

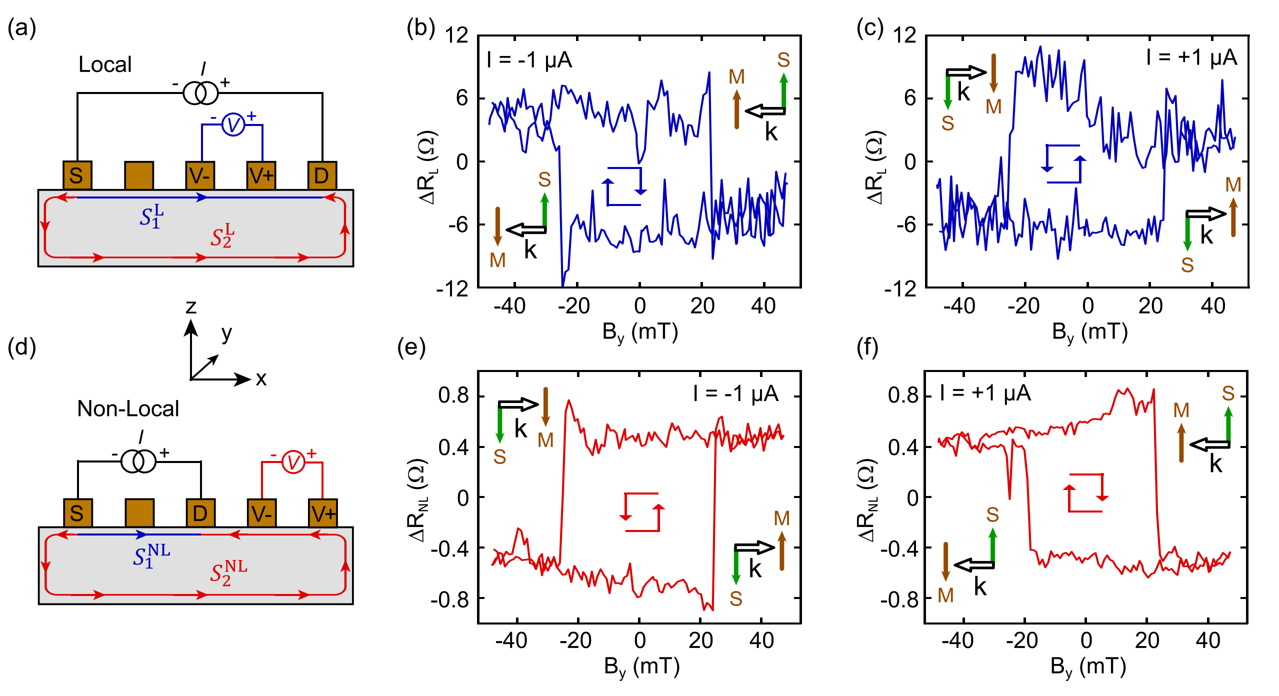

Figure 2. Schematic illustration of a) local and d) nonlocal measurement configurations. Potentiometric detection of the spin polarization in the TSS using b,c) local and e,f) nonlocal geometries at $T = 3$ K. The flow direction of electrons ($\vec{k}$) and their spin polarization direction ($\vec{S}$) assuming the spin-texture of the TSS are shown by black and green arrows, respectively. In-plane magnetization direction of the electrodes ($\vec{M}$) is indicated using the brown arrows. All measurements show a hysteretic switching of the spin signal when reversing the magnetization direction of the ferromagnetic detectors by an in-plane external magnetic field B_y.

conclusions as to whether the spin signal is due to transport via TSS or RSS. In many studies the sign of the hysteresis loop is used for this distinction.[8,9,13,16,19,22,24] However, as it was pointed out in other studies, the sign can also change depending on the resistance and characteristics of the electrical contacts,[15,21] making such an assignment ambiguous. This is aggravated in our case by the fact that not a single ferromagnetic contact is used with otherwise non-magnetic reference electrodes. If only ferromagnetic electrodes are used, the sign of the spin signal can in principle also change depending on the specific spin injection/detection efficiencies of the individual contacts.[15] We discuss both the experimental similarities and dissimilarities between TSS and RSS and the resulting problems in assigning the observed spin signal to one of these states in more detail in the Supporting Information.

Next we focus on the results of the NL measurements in Figure 2e,f. The amplitude of the spin signal of 1 Ω is around one order of magnitude smaller than in the local geometry, but still in the higher range of reported values in literature. Interestingly, we observe also a reversal of the hysteresis when comparing local and NL measurements for the same direction of the current between source and drain electrodes (compare respective upper and lower panels in Figure 2b,c,e,f. Under the assumption of similar spin detection efficiencies between the contacts, this sign reversal can be readily explained by a spin-polarized current through the bottom surface (see S_2^{NL} and red arrows in Figure 2d). As we kept the polarity of the voltage amplifier the same in both measurements geometries (first the negative input V_- then the positive input V_+ along the x-axis, compare Figure 2a,d), a current over S_2^{NL} will have a reversed current direction in the NL geometry (it flows from V_+ toward V_-) compared to the current over S_1^{L} in the local geometry (there it flows from V_- toward V_+). This results in a sign reversal and shows that the NL measurement allows to probe the surface currents flowing along the whole surface, i.e., from the top along the side to the bottom surface and back to the top surface along the opposite side.

However, there is one striking difference between the local and NL spin signals with respect to their magnetization independent background signals. Studies that conduct spin-sensitive measurements on TIs in the local detection geometry show background signals that are normally two to three orders of magnitude larger than the amplitude of the hysteresis signal.[8,13,16–20] These background signals are normally subtracted from the spin-dependent data, as we have done in Figure 2. The subtracted voltage signals are depicted in **Figure 3** as a function of the applied current for both the local (blue) and NL (red) geometry. The linear slope in the local geometry corresponds to a resistance of around 4.45 kΩ, which is in accordance to the temperature dependent data in Figure 1e. Therefore, the amplitudes of the local spin signals in Figure 2b,c are around a factor of 450 smaller than this background signal, which is in good agreement to literature values. Instead, the slope in the NL background signal in Figure 3, whose sign reversal compared to the local configuration is indicative for a current flow in the -x direction, corresponds to roughly 10 Ω. This background signal is only one order of magnitude larger than the NL spin signals in Figure 2e,f. To the best of our knowledge, this is the largest spin signal to background

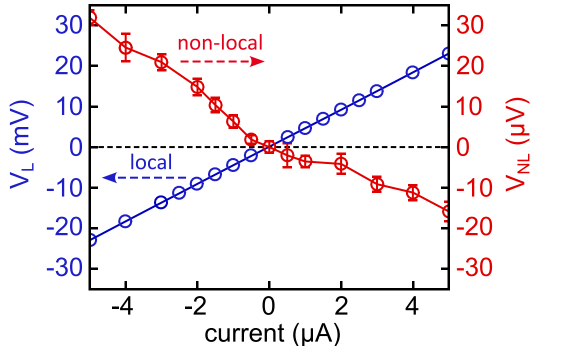

Figure 3. Nonmagnetization-dependent background signals in both local (blue) and nonlocal (red) configurations as a function of the applied current between source and drain contacts.

ratio in spin-sensitive electrical measurements on TIs reported in literature so far.

It should be noted that the ratio between spin signal to background signal in the NL geometry is not unreasonably large, but rather that the corresponding ratios in the local geometry are surprisingly low. If we assume that the spin polarization in the TSS is somewhere between 50% to 100%[53–57] and if we assume typical spin detection efficiencies of ferromagnetic contacts with tunnel barriers of around 10% to 30%,[58–61] one would expect that the nonmagnetization-dependent background would indeed be only one order of magnitude larger than the spin signal. Why the ratio in the local geometry is significantly lower not only in our study but also in other studies in literature (the aforementioned two to three orders of magnitude[8,13,16–20]) should be the focus of further studies.

Next, we discuss the temperature dependence of both the spin and background signals in both measurement geometries. **Figure 4**a,d are waterfall diagrams depicting the evolution of the hysteresis curves for both local and NL detection geometries with increasing temperature. The extracted amplitudes of the temperature dependent hysteresis curves are shown in Figure 4b,e, respectively. The magnetic field independent background signals are plotted in Figure 4c for the NL and 4(f) for the local geometry. There are two main observations in the temperature dependent measurements: First, the amplitude of the hysteresis in both configurations gets rapidly diminished as the temperature is increased. Interestingly, the NL spin signal already vanishes around $T = 16$ K (Figure 4b) while the local spin signal lasts up to $T = 45$ K (Figure 4e). Assuming that both signals originate from the same TSS or RSS states, we must link the different temperature dependencies to the different current paths (S_1^{L} and S_2^{NL} in Figure 2a,d, respectively).

In this respect, it is important that there is a distinct difference between the evolution of the background signals and the corresponding spin signals. In the NL geometry both quantities (ΔR_{NL} and R_{NL}) show a monotonic decrease and disappear at similar temperatures (Figure 4b,c). Instead, the background signal in the local geometry (R_L in Figure 4f) first slightly decreases from 3 to 10 K before it increases towards higher temperatures. Interestingly, the minimum of the local resistance in Figure 4f corresponds quite well with the temperature at which

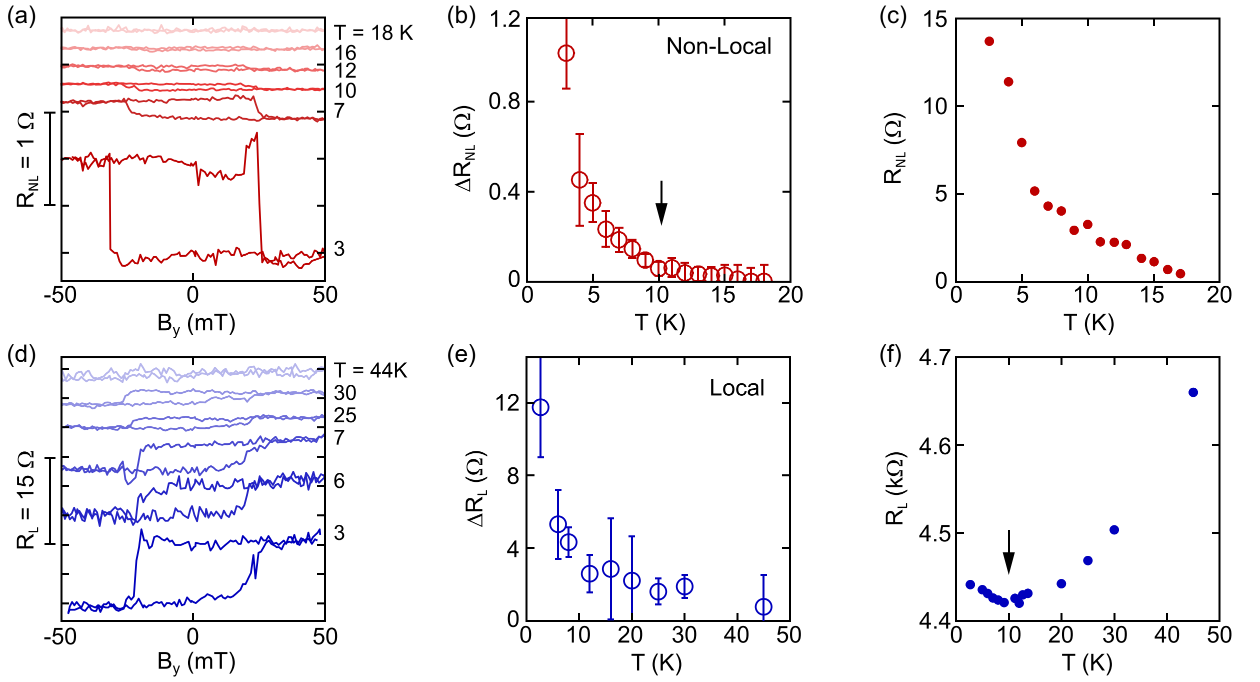

Figure 4. Temperature dependence of the a) nonlocal and d) local spin signals depicted as waterfall diagrams. Amplitudes of the spin signals in the b) nonlocal and e) local geometries as a function of temperature. The background signals on which the spin signal is superimposed in (a) and (d) are depicted in c) for the nonlocal and in f) for the local geometry by extracting the voltage values at $B = 50$ mT from (a) and (d) and normalizing these values by the applied current between the source and drain electrodes. The black arrows indicate the temperature at which the local voltage in panel (f) shows a minimum and the nonlocal spin signal in panel (b) disappears.

the NL spin signal in Figure 4b becomes very small (indicated by black arrows). As noted before, the local background signals extracted from the magnetic field dependent spin measurements (Figure 4f) follow the temperature dependent resistance measurement of Figure 1e. The latter reveals a transition from activated to metallic transport below $T = 200$ K, which indicates the depletion of bulk states. However, as it was shown previously, variable range hopping (VRH) in the bulk may still contribute to transport at low temperatures.[43,62] In particular, in BSTS compounds, the compensation of acceptors and donors, which can explain the low bulk carrier concentration, results in random local potential fluctuations and therefore the formation of charged puddles.[62] Charge carriers can tunnel between neighboring puddles and can therefore form a parallel conduction channel which couples to the surface states and gives rise to additional scattering of surface carriers. This mechanism can limit the spin-polarized transport on the surface and therefore can lead to a suppression of the NL signal.[63] We therefore argue that increasing the temperature toward 10 K activates hopping transport in the bulk, thereby shortening the NL current path S_2^{NL} in Figure 2d, which ultimately leads to a suppression of the NL spin signal at temperatures well below those relevant for the local transport geometry.

In conclusion, we have probed the spin-polarized surface states in BSTS by both local and NL spin-sensitive measurements. Our data suggest that the NL measurement allows to probe spin-polarized surface currents flowing along the whole surface, i.e., from the top along the side to the bottom surface and back to the top surface along the opposite side. This transport channel is suppressed at temperatures higher than 10 K most likely due to VRH over bulk states, which shortens the NL current path along the surface. Overall, our study demonstrates that at very low temperatures the NL surface currents of a TI in contact to an insulator (SiO_2 in our case) should to be taken into account in any spin transport measurement. Finally, we observe that the ratio between spin signal to background signal is almost two orders of magnitude higher in the NL geometry compared to the local one. In fact, the ratio in the NL geometry is in quite good agreement to typical spin detection efficiencies of ferromagnetic contacts with tunnel barriers and the expected spin polarization of the surface states. Accordingly, our study hints to the fact that so far a not well understood phenomena is diminishing the spin signal in the local geometry, which exact origin should be the subject of further studies.

Supporting Information

Supporting Information is available from the Wiley Online Library or from the author.

Acknowledgements

The authors gratefully acknowledge helpful discussions with M. Morgenstern. This project has received funding from the European Union's Horizon 2020 research and innovation programme under grant agreement no. 785219 and no. 881603 (Graphene Flagship) and no.

796388 (ECOMAT), the Virtual Institute for Topological Insulators (Jülich-Aachen-Würzburg-Shanghai), the Deutsche Forschungsgemeinschaft (DFG, German Research Foundation) under Germany's Excellence Strategy-Cluster of Excellence Matter and Light for Quantum Computing (ML4Q) EXC 2004/1-390534769 (Gefördert durch die Deutsche Forschungsgemeinschaft im Rahmen der Exzellenzstrategie des Bundes und der Länder - Exzellenzcluster Materie und Licht für Quanteninformation (ML4Q) EXC 2004/1 - 390534769), through DFG/SPP 1666 (BE 2441/8-2), and by the Helmholtz Nano Facility.[64] The work at Cologne was furthermore funded by the DFG under project no. 277146847-CRC 1238 (Subprojects A04)-and project no. 398945897.

Open Access funding enabled and organized by Projekt DEAL.

Conflict of Interest

The authors declare no conflict of interest.

Data Availability Statement

The data that support the findings of this study are available from the corresponding author upon reasonable request.

Keywords

nonlocal, spin transport, surface states, topological insulator

Received: June 10, 2025
Revised: October 6, 2025
Published online:

[1] M. Bianchi, D. Guan, S. Bao, J. Mi, B. B. Iversen, P. D. C. King, P. Hofmann, *Nat. Commun.* **2010**, *1*, 128.
[2] M. Michiardi, F. Boschini, H.-H. Kung, M. X. Na, S. K. Y. Dufresne, A. Currie, G. Levy, S. Zhdanovich, A. K. Mills, D. J. Jones, J. L. Mi, B. B. Iversen, P. Hofmann, A. Damascelli, *Nat. Commun.* **2022**, *13*, 3096.
[3] W. Ko, S.-H. Kang, J. Lapano, H. Chang, J. Teeter, H. Jeon, Q. Lu, A.-H. Chen, M. Brahlek, M. Yoon, R. G. Moore, A.-P. Li, *ACS Nano* **2024**, *18*, 18405.
[4] P. D. C. King, R. C. Hatch, M. Bianchi, R. Ovsyannikov, C. Lupulescu, G. Landolt, B. Slomski, J. H. Dil, D. Guan, J. L. Mi, E. D. L. Rienks, J. Fink, A. Lindblad, S. Svensson, S. Bao, G. Balakrishnan, B. B. Iversen, J. Osterwalder, W. Eberhardt, F. Baumberger, P. Hofmann, *Phys. Rev. Lett.* **2011**, *107*, 096802.
[5] M. Z. Hasan, C. L. Kane, *Rev. Mod. Phys.* **2010**, *82*, 3045.
[6] S. Hong, V. Diep, S. Datta, Y. P. Chen, *Phys. Rev. B* **2012**, *86*, 085131.
[7] Y. Ando, *J. Phys. Soc. Jpn.* **2013**, *82*, 102001.
[8] J. Tian, C. Sahin, I. Miotkowski, M. E. Flatté, Y. P. Chen, *Phys. Rev. B* **2021**, *103*, 035412.
[9] L. T. Dang, O. Breunig, Z. Wang, H. F. Legg, Y. Ando, *Phys. Rev. Appl.* **2023**, *20*, 024065.
[10] Q. L. He, T. L. Hughes, N. P. Armitage, Y. Tokura, K. L. Wang, *Nat. Mater.* **2022**, *21*, 15.
[11] O. Breunig, Y. Ando, *Reviews Physics* **2022**, *4*, 184.
[12] C. H. Li, J. Moon, O. M. J. van't Erve, D. Wickramaratne, E. D. Cobas, M. D. Johannes, B. T. Jonker, *ACS Appl. Mater. Interfaces* **2022**, *14*, 34093.
[13] J. Tian, I. Miotkowski, S. Hong, Y. P. Chen, *Sci. Rep.* **2015**, *5*, 14293.
[14] C. H. Li, O. M. J. van't Erve, S. Rajput, L. Li, B. T. Jonker, *Nat. Commun.* **2016**, *7*, 13518.
[15] C. H. Li, O. M. J. van't Erve, C. Yan, L. Li, B. T. Jonker, *Sci. Rep.* **2019**, *9*, 6906.
[16] C. H. Li, O. M. J. van't Erve, J. T. Robinson, Y. Liu, L. Li, B. T. Jonker, *Nat. Nanotechnol.* **2014**, *9*, 218.
[17] A. Dankert, J. Geurs, M. V. Kamalakar, S. Charpentier, S. P. Dash, *Nano Lett.* **2015**, *15*, 7976.
[18] J. Tang, L.-T. Chang, X. Kou, K. Murata, E. S. Choi, M. Lang, Y. Fan, Y. Jiang, M. Montazeri, W. Jiang, Y. Wang, L. He, K. L. Wang, *Nano Lett.* **2014**, *14*, 5423.
[19] Y. Ando, T. Hamasaki, T. Kurokawa, K. Ichiba, F. Yang, M. Novak, S. Sasaki, K. Segawa, Y. Ando, M. Shiraishi, *Nano Lett.* **2014**, *14*, 6226.
[20] T.-H. Hwang, H.-S. Kim, H. Kim, J. S. Kim, Y.-J. Doh, *Curr. Appl. Phys.* **2019**, *19*, 917.
[21] K. Vaklinova, K. Polyudov, M. Burghard, K. Kern, *J. Phys.: Condens. Matter* **2018**, *30*, 105302.
[22] A. Dankert, P. Bhaskar, D. Khokhriakov, I. H. Rodrigues, B. Karpiak, M. V. Kamalakar, S. Charpentier, I. Garate, S. P. Dash, *Phys. Rev. B* **2018**, *97*, 125414.
[23] J. S. Lee, A. Richardella, D. R. Hickey, K. A. Mkhoyan, N. Samarth, *Phys. Rev. B* **2015**, *92*, 155312.
[24] F. Yang, S. Ghatak, A. A. Taskin, K. Segawa, Y. Ando, M. Shiraishi, Y. Kanai, K. Matsumoto, A. Rosch, Y. Ando, *Phys. Rev. B* **2016**, *94*, 075304.
[25] D. Culcer, A. Cem Keser, Y. Li, G. Tkachov, *2D Mater.* **2020**, *7*, 022007.
[26] S. Majumder, K. Jarvis, S. K. Banerjee, K. L. Kavanagh, *J. Vacuum Sci. Technol. B* **2017**, *35*, 04F105.
[27] L. A. Walsh, C. M. Smyth, A. T. Barton, Q. Wang, Z. Che, R. Yue, J. Kim, M. J. Kim, R. M. Wallace, C. L. Hinkle, *J. Phys. Chem. C* **2017**, *121*, 23551.
[28] C. D. Spataru, F. M. C. Léonard, *Phys. Rev. B* **2014**, *90*, 085115.
[29] E. Longo, M. Belli, C. Wiemer, A. Lamperti, A. V. Matetskiy, P. M. Shevedyaeva, P. Moras, M. Fanciulli, R. Mantovan, *Nano Lett.* **2025**, *25*, 6888.
[30] W. Ko, G. D. Nguyen, H. Kim, J. S. Kim, X.-G. Zhang, A.-P. Li, *Phys. Rev. Lett.* **2018**, *121*, 176801.
[31] G. M. Stephen, I. Naumov, S. Tyagi, O. A. Vail, J. E. DeMell, M. Dreyer, R. E. Butera, A. T. Hanbicki, P. J. Taylor, I. Mayergoyz, P. Dev, A. L. Friedman, *J. Phys. Chem. C* **2020**, *124*, 27082.
[32] S. N. Shirodkar, G. M. Stephen, A. T. Hanbicki, A. L. Friedman, P. Dev, *J. Phys. Chem. C* **2022**, *126*, 16877.
[33] N. P. Stepina, A. O. Bazhenov, A. V. Shumilin, A. Y. Kuntsevich, V. V. Kirienko, E. S. Zhdanov, D. V. Ishchenko, O. E. Tereshchenko, *Phys. Rev. B* **2023**, *108*, 115401.
[34] S. Sasmal, J. Mukherjee, D. Suri, K. V. Raman, *J. Phys.: Condens. Matter* **2021**, *33*, 465601.
[35] S. Jafarpisheh, A. Ju, K. Janßen, T. Taniguchi, K. Watanabe, C. Stampfer, B. Beschoten, *Phys. Status Solidi B* **2021**, *258*, 2000021.
[36] A. Y. Kuntsevich, A. V. Shupletsov, G. M. Minkov, *Phys. Rev. B* **2018**, *97*, 195431.
[37] E. K. de Vries, A. M. Kamerbeek, N. Koirala, M. Brahlek, M. Salehi, S. Oh, B. J. van Wees, T. Banerjee, *Phys. Rev. B* **2015**, *92*, 201102.
[38] L. Fu, C. L. Kane, E. J. Mele, *Phys. Rev. Lett.* **2007**, *98*, 106803.
[39] S. Wolgast, Ç. Kurdak, K. Sun, J. W. Allen, D.-J. Kim, Z. Fisk, *Phys. Rev. B* **2013**, *88*, 180405.
[40] D. J. Kim, S. Thomas, T. Grant, J. Botimer, Z. Fisk, J. Xia, *Sci. Rep.* **2013**, *3*, 3150.
[41] C. Shekhar, C. E. ViolBarbosa, B. Yan, S. Ouardi, W. Schnelle, G. H. Fecher, C. Felser, *Phys. Rev. B* **2014**, *90*, 165140.
[42] J. Lee, J.-H. Lee, J. Park, J. S. Kim, H.-J. Lee, *Phys. Rev. X* **2014**, *4*, 011039.
[43] Z. Ren, A. A. Taskin, S. Sasaki, K. Segawa, Y. Ando, *Phys. Rev. B* **2011**, *84*, 165311.

[44] Z. Ren, A. A. Taskin, S. Sasaki, K. Segawa, Y. Ando, *Phys. Rev. B* **2010**, *82*, 241306.
[45] S.-P. Chiu, J.-J. Lin, *Phys. Rev. B* **2013**, *87*, 035122.
[46] H.-Z. Lu, S.-Q. Shen, *Phys. Rev. B* **2011**, *84*, 125138.
[47] H.-Z. Lu, J. Shi, S.-Q. Shen, *Phys. Rev. Lett.* **2011**, *107*, 076801.
[48] Y. S. Kim, M. Brahlek, N. Bansal, E. Edrey, G. A. Kapilevich, K. Iida, M. Tanimura, Y. Horibe, S.-W. Cheong, S. Oh, *Phys. Rev. B* **2011**, *84*, 073109.
[49] D. Kim, P. Syers, N. P. Butch, J. Paglione, M. S. Fuhrer, *Nat. Commun.* **2013**, *4*, 2040.
[50] S. Hikami, A. I. Larkin, Y. Nagaoka, *Progr. Theor. Phys.* **1980**, *63*, 707.
[51] R. Ockelmann, A. Müller, J. H. Hwang, S. Jafarpisheh, M. Drögeler, B. Beschoten, C. Stampfer, *Phys. Rev. B* **2015**, *92*, 085417.
[52] F. Volmer, M. Drögeler, E. Maynicke, N. von den Driesch, M. L. Boschen, G. Güntherodt, C. Stampfer, B. Beschoten, *Phys. Rev. B* **2014**, *90*, 165403.
[53] O. V. Yazyev, J. E. Moore, S. G. Louie, *Phys. Rev. Lett.* **2010**, *105*, 266806.
[54] Z.-H. Zhu, C. N. Veenstra, G. Levy, A. Ubaldini, P. Syers, N. P. Butch, J. Paglione, M. W. Haverkort, I. S. Elfimov, A. Damascelli, *Phys. Rev. Lett.* **2013**, *110*, 216401.
[55] M. Morgenstern, C. Pauly, J. Kellner, M. Liebmann, M. Pratzer, G. Bihlmayer, M. Eschbach, L. Plucinski, S. Otto, B. Rasche, M. Ruck, M. Richter, S. Just, F. Lüpke, B. Voigtländer, *Phys. Status Solidi B* **2021**, *258*, 2000060.
[56] C. Jozwiak, J. A. Sobota, K. Gotlieb, A. F. Kemper, C. R. Rotundu, R. J. Birgeneau, Z. Hussain, D.-H. Lee, Z.-X. Shen, A. Lanzara, *Nat. Commun.* **2016**, *7*, 13143.
[57] C. Pauly, G. Bihlmayer, M. Liebmann, M. Grob, A. Georgi, D. Subramaniam, M. R. Scholz, J. Sán, chez-Barriga, A. Varykhalov, S. Blügel, O. Rader, M. Morgenstern, *Phys. Rev. B* **2012**, *86*, 235106.
[58] E. C. Ahn, *Npj 2D Mater. Appl.* **2020**, *4*, 17.
[59] W. Han, K. McCreary, K. Pi, W. Wang, Y. Li, H. Wen, J. Chen, R. Kawakami, *J. Magn. Magn. Mater.* **2012**, *324*, 369.
[60] W. Han, K. Pi, K. M. McCreary, Y. Li, J. J. I. Wong, A. G. Swartz, R. K. Kawakami, *Phys. Rev. Lett.* **2010**, *105*, 167202.
[61] M. Popinciuc, C. Józsa, P. J. Zomer, N. Tombros, A. Veligura, H. T. Jonkman, B. J. van Wees, *Phys. Rev. B* **2009**, *80*, 214427.
[62] B. Skinner, T. Chen, B. I. Shklovskii, *Phys. Rev. Lett.* **2012**, *109*, 176801.
[63] H. Velkov, G. N. Bremm, T. Micklitz, G. Schwiete, *Phys. Rev. B* **2018**, *98*, 165408.
[64] W. Albrecht, J. Moers, B. Hermanns, *JLSRF* **2017**, *3*, 112.